

Hadroproduction of neutral K^* -mesons up to LHC energies

G.H. Arakelyan¹, C. Merino², Yu.M. Shabelski³

¹A.Alikhanyan National Scientific Laboratory
(Yerevan Physics Institute)
Yerevan, 0036, Armenia
e-mail: argev@mail.yerphi.am

²Departamento de Física de Partículas, Facultade de Física
and Instituto Galego de Física de Altas Enerxías (IGFAE)
Universidade de Santiago de Compostela
15782 Santiago de Compostela
Galiza-Spain
e-mail: carlos.merino@usc.es

³Petersburg Nuclear Physics Institute
NCR Kurchatov Institute
Gatchina, St.Petersburg 188350, Russia
e-mail: shabelsk@thd.pnpi.spb.ru

Abstract

We consider the experimental data on neutral K^* -meson production on nucleon and nuclear targets. The Quark-Gluon String Model quantitatively describes the inclusive density in the midrapidity region, as well as the initial energy and A dependences of the produced K^* -mesons.

1 Introduction

The study of resonance production plays an important role in collisions with nucleon as well as nuclear targets. In pp collisions it contributes to the understanding of hadron production, as the decay products of resonances represent a large fraction of the final state particles.

An useful probe of strangeness production is the $K^{*0}(892)$, which is a vector meson with a mass similar to that of the φ -meson, but with a strangeness quantum number differing by one unit of that of the φ -meson.

The very short lifetime and the strange valence quark content of the K^* -meson make the K^* -meson production process sensitive to the properties of the dense matter and of strangeness production, from an early partonic phase. Thus, the measurement of K^* -meson properties, such as mass, width, and yields can provide significant insight on the dynamics in the dense medium created in heavy-ion collisions.

The hadroproduction of vector φ -mesons in the frame of Quark-Gluon String Model (QGSM) [1, 2] was considered in [3, 4].

In this paper we extend the investigation of vector meson production to the case of K^{*0} and \bar{K}^{*0} -meson spectra in proton-proton, proton-nucleus, and nucleus-nucleus collisions, for a wide range of the initial energy, going up from that of the NA49 experiment, to current the RHIC and LHC energies.

The QGSM is based on the Dual Topological Unitarization (DTU), Regge phenomenology, and nonperturbative notions of QCD, and it has been used for the description of secondary particle production at high energies. In particular, the QGSM provides quantitative predictions on the inclusive densities of different secondaries in the central and beam fragmentation regions in hadron-nucleon [1, 2], hadron-nucleus [5, 6], and nucleus-nucleus [7, 8] collisions.

The description of the production of secondary pseudoscalar mesons π and K , and of baryons p , \bar{p} , Λ , and $\bar{\Lambda}$, was obtained in [9, 10, 11, 12]), while vector meson production was considered in [3, 4, 13, 14].

The experimental data on neutral K^{*0} and \bar{K}^{*0} -mesons produced by pion and proton beams on proton target [15, 16] at not very high energies was already considered in [17].

In the case of collisions on a nuclear target, a new effect was discovered at very high energies, namely the saturation of inclusive density of secondaries [18, 19, 20]. This saturation effect is also successfully described by QGSM [20, 21, 22].

2 Meson inclusive spectra in the QGSM

In order to produce quantitative results for the inclusive spectra of secondary hadrons, a model for multiparticle production is needed. It is for that purpose that we have used the QGSM [1, 2] in the numerical calculations presented below.

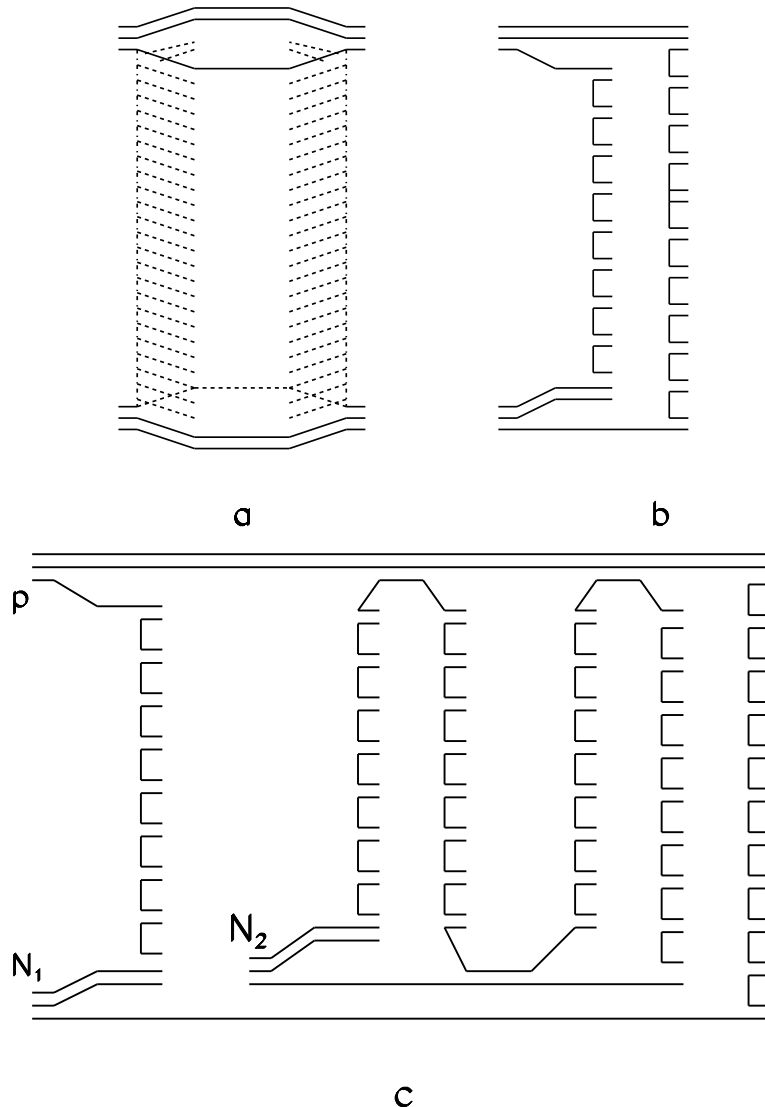


Figure 1: (a) Cylindrical diagram representing the Pomeron exchange within the Dual Topological Unitarization (DTU) classification (quarks are shown by solid lines); (b) Cut of the cylindrical diagram corresponding to the single-Pomeron exchange contribution in inelastic pp scattering; (c) Diagram corresponding to the inelastic interaction of an incident proton with two target nucleons N_1 and N_2 in a pA collision.

In the QGSM, the high energy hadron-nucleon, hadron-nucleus, and nucleus-nucleus interactions are treated as proceeding via the exchange of one or several Pomerons, and all elastic and inelastic processes result from cutting through or between Pomerons [23].

Each Pomeron corresponds to a cylinder diagram (see Fig. 1a), in which the cylinder boundaries are drawn by the dash-dotted vertical lines. The surface of the cylinder is schematically depicted by dashed lines, while the solid lines at the top and bottom of the cylinder represent, respectively, the beam and the target quarks, which interaction is mediated by the Pomeron exchange.

The cut through the cylinder produces two showers of secondaries, i.e. quark-antiquark pairs shown in Fig 1b by solid lines. The inclusive spectrum of secondaries is then determined by the convolution of diquark, valence quark, and sea quark distributions in the incident particles, $u(x, n)$, with the fragmentation functions of quarks and diquarks into the secondary hadrons, $G(z)$. Both functions $u(x, n)$ and $G(z)$ are determined by the appropriate Reggeon diagrams [24].

Note that the quark (antiquark) distributions $u(x, n)$ ($u(\bar{x}, n)$) differ from the standard PDF's extracted from fits to experimental data because theoretically they are taken to be valid at the rather low Q^2 relevant for soft processes, while the PDF distributions are obtained by fixing the behaviour at large Q^2 . The diquark and quark distribution functions depend on the number n of cut Pomerons in the considered diagram. In the following calculations we have used the prescription given in reference [5].

For a nucleon target, the inclusive rapidity, y , or Feynman- x , x_F , spectrum of a secondary hadron h has the form [1, 2]:

$$\frac{dn}{dy} = \frac{x_E}{\sigma_{inel}} \cdot \frac{d\sigma}{dx_F} = \sum_{k=1}^{\infty} w_k \cdot \phi_k^h(x) , \quad (1)$$

where $x_E = E/E_{max}$, is the relative energy of the secondary particle, the functions $\phi_k^h(x)$ determine the contribution of diagrams with k cut Pomerons, and w_k is the relative weight of this diagram, determined as

$$w_k = \sigma_k / (\sigma_{tot} - \sigma_{el}) , \quad (2)$$

Here, for the production of K^* -mesons, we neglect by the contribution of diffraction and dissociation processes.

In the case of pp collisions:

$$\begin{aligned} \phi_k^h(x) &= f_{qq}^h(x_+, k) \cdot f_q^h(x_-, k) + f_q^h(x_+, k) \cdot f_{qq}^h(x_-, k) \\ &+ 2(k-1) \cdot f_s^h(x_+, k) \cdot f_s^h(x_-, k) , \end{aligned} \quad (3)$$

$$x_{\pm} = \frac{1}{2} [\sqrt{4m_T^2/s + x^2} \pm x] , \quad (4)$$

where $m_T = \sqrt{m^2 + p_T^2}$ is the transverse mass of the produced hadrons, and f_{qq} , f_q , and f_s correspond to the contributions of diquarks, valence quarks, and sea quarks, respectively. The contribution of sea quarks and sea antiquarks are assumed to be equal, the difference between quarks and antiquarks being the valence quarks contribution [2, 24].

These contributions are determined by the convolution of the diquark and quark distributions with the fragmentation functions, e.g.,

$$f_i^h(x_{\pm}, k) = \int_{x_{\pm}}^1 u_i(x_1, k) G_i^h(x_{\pm}/x_1) dx_1 \quad , \quad (5)$$

where $i = qq$ -diquarks, valence q, \bar{q} , and sea quarks.

In this paper we have used the distribution functions in the colliding particles of valence and sea quarks, and of diquarks, obtained in [2, 3, 10, 25].

For the case of meson production, one has the diagram corresponding to quark and diquark fragmentation to secondary mesons shown in Fig. 2:

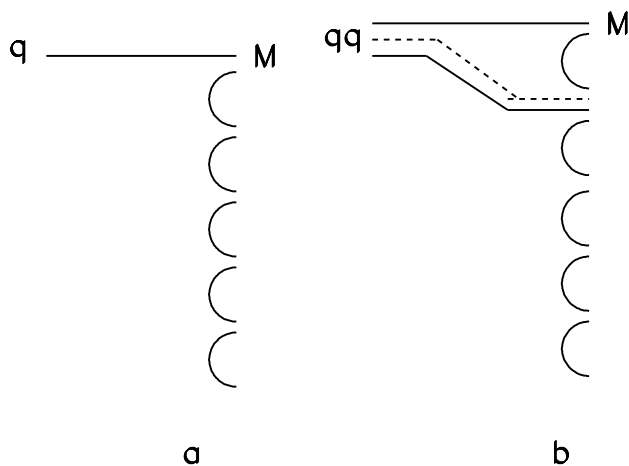


Figure 2: QGSM diagrams corresponding to fragmentation of (a) quark and (b) diquark into a secondary meson M .

As for the fragmentation function of quarks and diquarks into neutral vector mesons K^{*0} and \bar{K}^{*0} , $G_{q,qq}^{K^*}(z)$, we have used the corresponding fragmentation functions for pseudoscalar K -meson production given in ref. [10, 25]. These fragmentation functions were obtained using the Reggeon counting rules and the simplest extrapolation [2, 24]. The question of spin dependence of fragmentation functions was analyzed in the paper [17]. Following this paper, we assume that the functional form of the fragmentation functions is spin independent, the spin dependence only appearing in the value of the normalisation parameter a^{K^*} (see below in this section).

With these assumptions, the quark/antiquark fragmentation functions $G_q^{K^*}(z)$ can be written as:

$$\begin{aligned} G_d^{K^{*0}}(z) &= a^{K^*} (1-z)^{-\alpha_\varphi(0)+\lambda} (1+b_1^K z) \quad , \\ G_d^{\bar{K}^{*0}}(z) &= G_u^{\bar{K}^{*0}}(z) = a^{K^*} (1-z)^{-\alpha_\varphi(0)+\lambda+1} \quad , \end{aligned}$$

$$\begin{aligned}
G_{\bar{s}}^{K^*0}(z) &= G_{\bar{s}}^{\bar{K}^*0}(z) = bz^{1-\alpha_\varphi(0)}(1-z)^{-\alpha_R(0)+\lambda} + \\
&+ a^{K^*}(1-z)^{-\alpha_R(0)+\lambda+2(1-\alpha_\varphi(0))} , \\
G_{\bar{s}}^{\bar{K}^*0}(z) &= G_s^{K^*0}(z) = a^{K^*}(1-z)^{-\alpha_R(0)+\lambda+2(1-\alpha_\varphi(0))} .
\end{aligned} \tag{6}$$

Correspondingly, the fragmentation functions for diquarks, $G_{qq}^{K^*}(z)$, are:

$$\begin{aligned}
G_{uu}^{\bar{K}^*0}(z) &= G_{uu}^{K^*0}(z) = a^{K^*}(1-z)^{-\alpha_\varphi(0)-2\alpha_N(0)+\lambda+2} , \\
G_{ud}^{\bar{K}^*0}(z) &= a^{K^*}(1-z)^{-\alpha_\varphi(0)-2\alpha_N(0)+\lambda+2}(1-z/2) , \\
G_{ud}^{K^*0}(z) &= a^{K^*}(1-z)^{-\alpha_\varphi(0)-2\alpha_N(0)+\lambda+2}(1+b_2^K z/2) ,
\end{aligned} \tag{7}$$

where $\alpha_\varphi(0) \approx 0$, $b_1^K \approx 2$, $b_2^K \approx 5$, and $b \approx 0.4$.

The parameter $\lambda = 2\alpha'_R < p_\perp^2 >_{K^*}$, with $\alpha'_R \approx 1$ is the slope of the vector Regge trajectory, and $< p_\perp^2 >_{K^*}$ is the average transverse squared momenta of the produced meson.

In ref. [17], the relations for the probabilities of the production of the light and strange pseudoscalar and vector mesons were obtained, by using the predictions of the resonance decay model [26].

The normalization parameter a_K^* in the fragmentation functions of eqs. (6) and (7) is related to parameter a_K , earlier determined in QGSM for the description of K -meson production [9, 10], by the equation:

$$(a^{K^*}/a^K)^2 = \frac{< k_\perp^2 >_K}{4m_q^2} , \tag{8}$$

where $m_q = 0.415 \pm 0.015$ is the transverse mass of the constituent quark [26]. Taking into account that $< k_\perp^2 >_K \approx 0.21 \text{ GeV}^2$, and $a_K \approx 0.27$ [9, 10], we find

$$a^{K^*} \approx 0.15 . \tag{9}$$

In the calculation of the inclusive spectra of secondaries produced in pA collisions we should consider the possibility of one or several Pomeron cuts in each of the ν blobs of the proton-nucleon inelastic interactions. For example, in Fig. 1c it is shown one of the diagrams contributing to the inelastic interaction of a beam proton with two nucleons from the target. In the blob of the proton-nucleon₁ interaction one Pomeron is cut, and in the blob of the proton-nucleon₂ interaction two Pomerons are cut.

The contribution of the diagram in Fig. 1c to the inclusive spectrum is presented in refs. [3, 6, 27].

The total number of exchanged Pomerons becomes as large as

$$\langle k \rangle_{pA} \sim \langle \nu \rangle_{pA} \cdot \langle k \rangle_{pN} , \tag{10}$$

where $\langle \nu \rangle_{pA}$ is the average number of inelastic collisions inside the nucleus (about 4 for heavy nuclei at fixed target energies).

The process shown in Fig. 1c satisfies [28, 29, 30, 31] the condition that the absorptive parts of the hadron-nucleus amplitude are determined by the combination of the absorptive parts of the hadron-nucleon amplitudes.

In the case of a nucleus-nucleus collision, in the projectile fragmentation region we use the approach [7, 27, 32], with the beam of independent nucleons of the projectile interacting with the target nucleus, what corresponds to the rigid target approximation [33] of the Glauber Theory. In the target fragmentation region, on the contrary, the beam of independent target nucleons interact with the projectile nucleus, the two approaches coinciding in the central region. The corrections due to energy conservation play here a very important role when the initial energy is not very high.

3 Neutral K^* mesons production in pp collisions

In Fig. 3 we compare the experimental data of NA49 Collaboration [34] on the rapidity dependence of dn/dy density of K^{*0} and \bar{K}^{*0} production in pp collisions at 158 GeV/c with the results of the QGSM calculations. The full dots and triangles represent the measured experimental data on K^{*0} and \bar{K}^{*0} , respectively.

Here the theoretical curves are only shown for the rapidity region $y^* \geq 0$, where the experimental data were measured, and we omit them in the negative y^* region where NA49 presents the mirror reflection data.

As it can be seen in Fig. 3, the agreement between the theoretical curve and the experimental data is rather good for \bar{K}^{*0} -meson production in the whole experimental region, while For K^{*0} -meson production the theoretical curve is slightly lower than the experimental points.

In Fig. 4, we compare the results of the QGSM calculations for the x_F -spectra $d\sigma/dx_F$ of K^{*0} (full curve) and \bar{K}^{*0} (dashed curve) mesons produced in pp collisions at 400 GeV/c, with the corresponding experimental data by the LEBC-EHS Collaboration [35]. The comparison of the theoretical curves with the experimental data provides a reasonable agreement for the whole measured x_F range.

The energy dependence of the density dn/dy ($y = 0$) of neutral strange mesons produced in pp collisions is shown in Fig. 5. Since the experimental data from RHIC and those by the ALICE Collaboration were presented for average $(K^{*0} + \bar{K}^{*0})/2$ mesons, here we also plot the NA49 Collaboration data for the average K^{*0} meson. The results of the model calculation show to be in agreement with the experimental data.

In the Table 1 we present the experimental data on the densities of neutral K^* -mesons produced in pp collisions for energy region ranging from the NA49 Collaboration to LHC. Note that the NA49 experiment separately measured K^{*0} and \bar{K}^{*0} mesons, while at RHIC and the ALICE Collaboration at LHC the average density of neutral

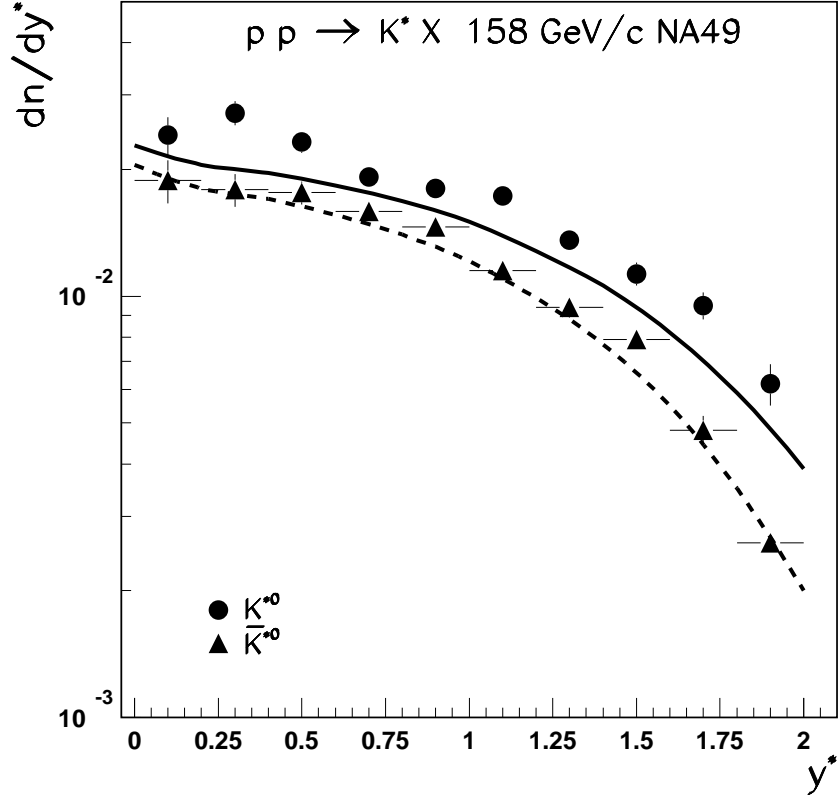


Figure 3: Comparison of the results of the QGSM calculations for the y -dependence dn/dy of K^{*0} (full line) and \bar{K}^{*0} (dashed line) mesons produced in pp collisions at 158 GeV/c, with the corresponding experimental data by the NA49 Collaboration [34].

K^* mesons $(K^{*0} + \bar{K}^{*0})/2$ was measured.

Reaction	Produced particle	Energy \sqrt{s} (GeV)	Experimental data dn/dy $ y \leq 0.5$	QGSM
$p + p$	K^{*0}	17.3	$0.0257 \pm 0.0031 \pm 0.0023$ [34]	0.0228
$p + p$	\bar{K}^{*0}	17.3	$0.0183 \pm 0.0027 \pm 0.0016$ [34]	0.0205
$p + p$	$(K^{*0} + \bar{K}^{*0})/2$	200.0	$0.0508 \pm 0.0017 \pm 0.0061$ [36]	0.0443
$p + p$	$(K^{*0} + \bar{K}^{*0})/2$	2760.0	$0.0705 \pm 0.0007 \pm 0.009$ [37]	0.0755
$p + p$	$(K^{*0} + \bar{K}^{*0})/2$	7000.0	$0.097 \pm 0.00004 \pm 0.01$ [38]	0.106

Table 1: Experimental data on dn/dy , $|y| \leq 0.5$, of neutral K^* -mesons production in pp collisions at different energies, together with the results of the corresponding QGSM calculations.

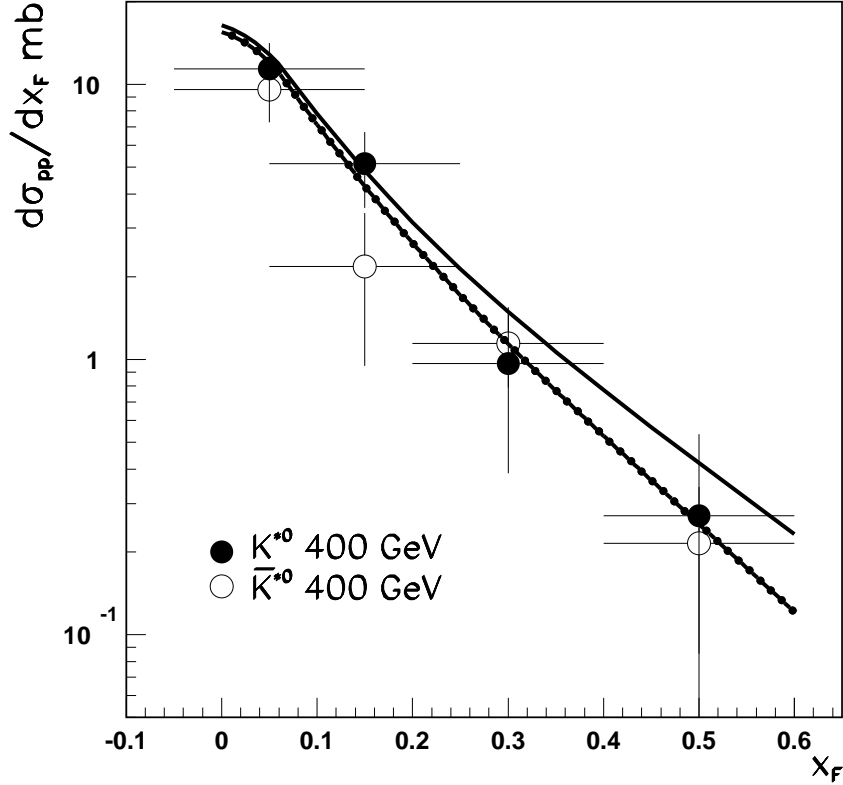


Figure 4: Comparison of the results of the QGSM calculations for the x_F -spectra $d\sigma/dx_F$ of K^{*0} (full curve) and \bar{K}^{*0} (dashed curve) mesons produced in pp collisions at 400 GeV/c, with the corresponding experimental data by the LEBC-EHS Collaboration [35].

4 K^* -meson production on nuclear targets at not very high energies

In this section we consider K^{*0} and \bar{K}^{*0} meson production in proton and nucleus collisions on nuclear targets at the energies of NA49, HERAb, and RHIC.

In Fig. 6 we compare the results of the QGSM calculations for the rapidity spectra dn/dy of K^{*0} (full line) and \bar{K}^{*0} (dashed line) mesons produced in Pb+Pb collisions at 158 GeV/c, with the corresponding experimental data by the NA49 Collaboration [34]. As it can be seen in the figure, the agreement is reasonable for the case \bar{K}^{*0} production, while for K^{*0} production the theoretical curve is slightly lower than experiment.

The experimental data on the inclusive cross section rapidity distribution, $d\sigma/dy^*$, for K^{*0} and \bar{K}^{*0} meson production in proton collisions with different nuclei, measured by the HERAb Collaboration [39] at $\sqrt{s} = 41.6$ GeV are compared in Fig. 7 with the results of the QGSM calculations. The agreement appears to be rather good.

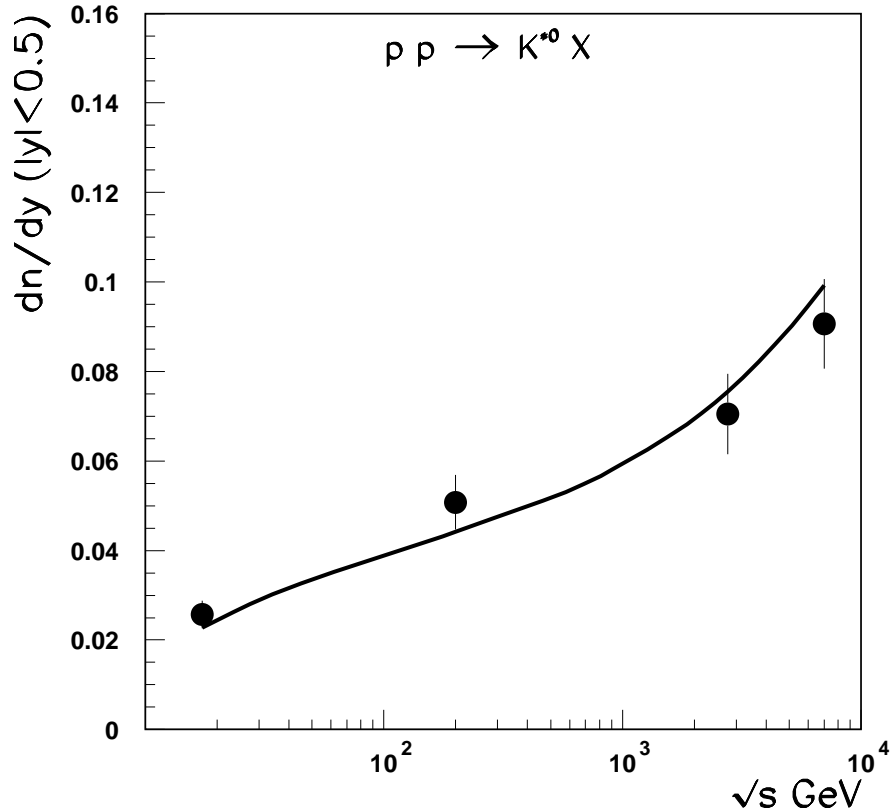


Figure 5: Comparison of the experimental data [34, 36, 38] on the \sqrt{s} -dependence of the density $dn/dy(|y| < 0.5)$ of average $(K^{*0} + \bar{K}^{*0})/2$ mesons produced in pp collisions, with the results of the corresponding QGSM calculations.

In Fig. 8 we compare the experimental data by the HERAb Collaboration on the atomic number A dependence of K^{*0} and \bar{K}^{*0} meson production in pA collisions at $\sqrt{s} = 41.6$ GeV [39], with the corresponding QGSM predictions. The solid curve shows the K^{*0} -meson production. The curve for \bar{K}^{*0} -mesons production practically coincides with the curve for K^{*0} , and so it is not shown.

In Table 2 we compare the corresponding results of QGSM calculations with the experimental data by the HERAb Collaboration [39] on the cross section σ_{vis} (mb)

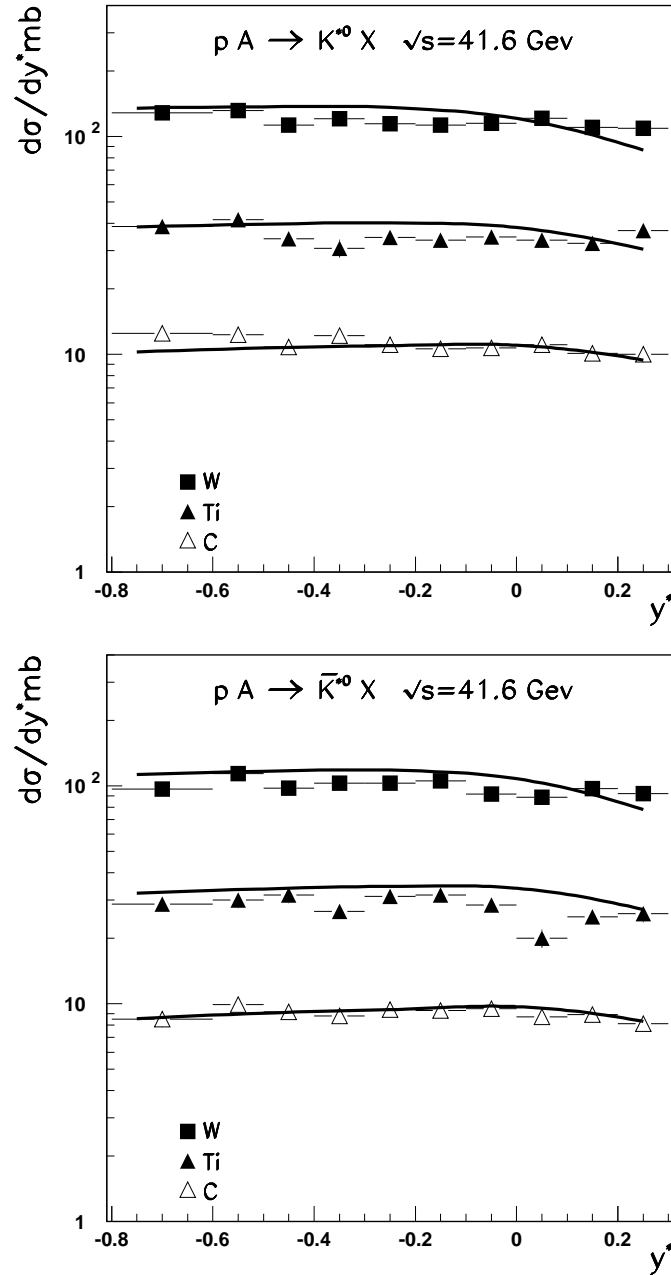


Figure 6: Comparison of the results of QGSM calculations for the y -spectra $d\sigma/dy$ of K^{*0} (upper panel) and \bar{K}^{*0} (lower panel) mesons produced in proton-nucleus collisions on different nuclear targets at $\sqrt{s} = 41.6$ GeV, with the corresponding experimental data for nuclear targets C , Ti , and W [39].

measured in a rather short rapidity region $-0.75 \leq y \leq 0.25$, and with the results of the extrapolation of data on K^{*0} and \bar{K}^{*0} meson production cross section σ_{prod} (mb) for the whole rapidity region. The theoretical results for the cross section σ_{prod} are lower than the experimental data. This can be connected with a different behaviour of the theoretical curves and the experimental extrapolations in the whole rapidity region. On the other hand, the theoretical results for σ_{vis} consistently coincide with the experimental measurements.

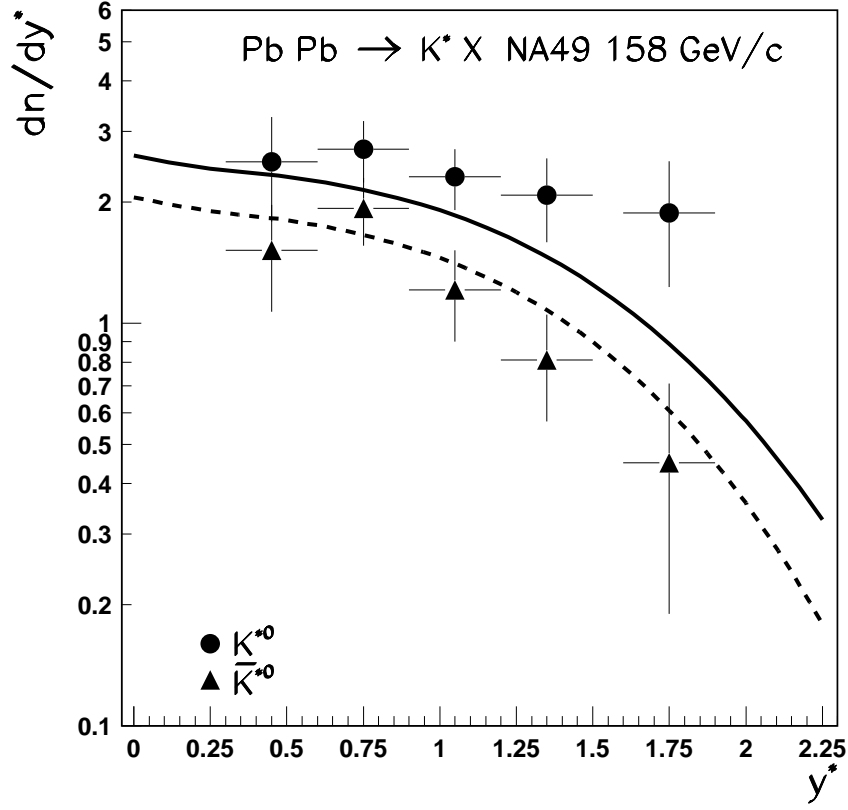


Figure 7: Comparison of the results of the QGSM calculations for the rapidity spectra dn/dy^* of K^{*0} (full line) and \bar{K}^{*0} (dashed line) mesons produced in Pb+Pb collisions at 158 GeV/c, with the corresponding experimental data by the NA49 Collaboration [34].

Reaction ($\sqrt{s} = 41.6 \text{ GeV}$)	Produced particle	Experimental data $\sigma_{pA}^{prod} \text{ mb}$	$\sigma_{vis}(\text{mb})$	QGSM total	QGSM visible
$p + C$	K^{*0}	$43.9 \pm 0.6 \pm 3.3$	$12.1 \pm 0.2 \pm 0.9$	36.24	15.03
$p + Ti$	K^{*0}	$141.2 \pm 2.6 \pm 10.6$	$38.5 \pm 0.7 \pm 2.7$	124.74	46.07
$p + W$	K^{*0}	$465.9 \pm 6.4 \pm 32.7$	$127.5 \pm 1.7 \pm 8.3$	402.03	153.86
$p + C$	\bar{K}^{*0}	$36.0 \pm 0.6 \pm 2.9$	$10.0 \pm 0.2 \pm 0.7$	29.04	11.25
$p + Ti$	\bar{K}^{*0}	$111.5 \pm 2.5 \pm 9.7$	$31.1 \pm 0.7 \pm 2.3$	100.03	40.34
$p + W$	\bar{K}^{*0}	$388.8 \pm 6.9 \pm 30.8$	$107.6 \pm 1.9 \pm 7.0$	318.52	133.34

Table 2: Comparison of the results of the QGSM calculations for K^{*0} and \bar{K}^{*0} meson production σ_{prod} and for visible σ_{vis} cross sections in pA collisions with the corresponding experimental data by the HERAb Collaboration at $\sqrt{s} = 41.6 \text{ GeV}$ [39].

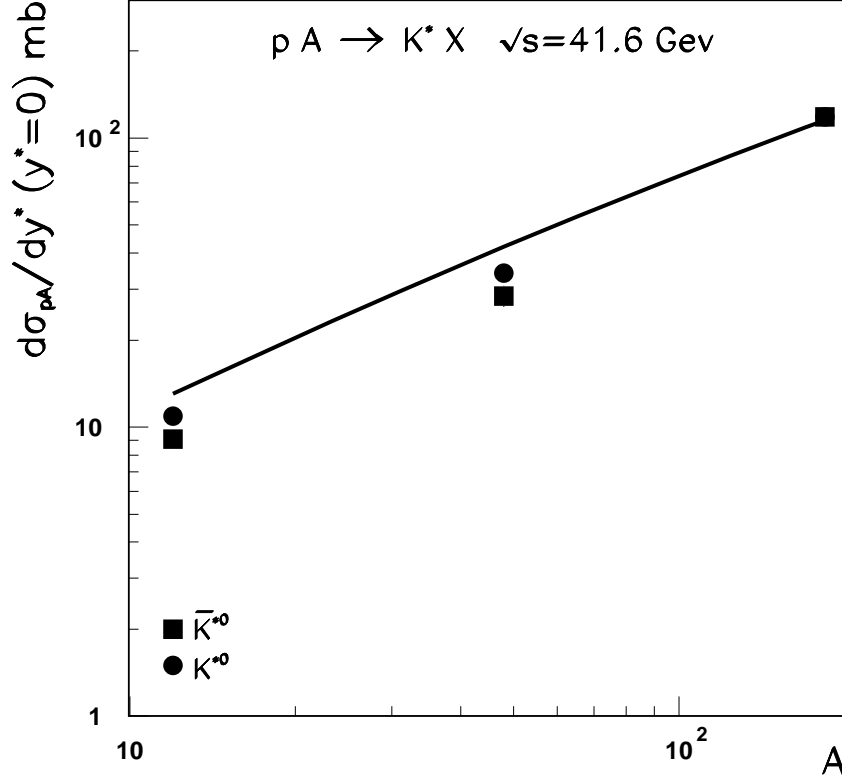


Figure 8: Comparison of the results of QGSM calculations for the A -dependence of K^{*0} (solid line) and \bar{K}^{*0} meson production in pA collisions at $\sqrt{s} = 41.6 \text{ GeV}$ with the corresponding experimental data by the HERAb Collaboration [39]. The curve representing the QGSM prediction for \bar{K}^{*0} -meson production practically coincides with the solid curve for K^{*0} , and so it is not shown.

Reaction	Centrality	Energy $\sqrt{s} \text{ (GeV)}$	Experimental data $dn/dy, y \leq 0.5$	QGSM
$Au + Au \rightarrow K^{*0} + X$	0 - 20%	62.4	$6.4 \pm 0.4 \pm 0.7$ [40]	5.97
$Au + Au \rightarrow K^{*0} + X$	0 - 5%	130.0	10.0 ± 0.9 [41]	9.25
$Au + Au \rightarrow K^{*0} + X$	min. bias	130.0	$4.5 \pm 0.7 \pm 1.4$ [41]	2.52
$Au + Au \rightarrow K^{*0} + X$	0 - 109	200.0	$10.48 \pm 1.45 \pm 1.94$ [36]	9.83
$Au + Au \rightarrow K^{*0} + X$	0 - 10%	200.0	$9.05 \pm 0.57 \pm 1.01$ [40]	9.83
$Cu + Cu \rightarrow K^{*0} + X$	0 - 20%	200.0	$2.96 \pm 0.12 \pm 0.3$ [40]	2.9

Table 3: Experimental data on $dn/dy, |y| \leq 0.5$, of average neutral $K^{*0} = (K^{*0} + \bar{K}^{*0})/2$ meson production in different central nucleus-nucleus collisions at RHIC energies, together with the results of the corresponding QGSM calculations.

In Table 3 the experimental data on the inclusive densities dn/dy for average $K^{*0}=(K^{*0} + \bar{K}^{*0})/2$ mesons produced at RHIC (STAR Collaboration, $\sqrt{s} = 62.4$ GeV [40], $\sqrt{s} = 130$ GeV [41], and $\sqrt{s} = 200$ GeV [36, 40]) in the midrapidity region for different nucleus-nucleus collisions, are compared with the results of the corresponding QGSM calculations.

The QGSM predictions presented in this section show that the inelastic shadowing effects for neutral vector K^* -meson production are very weak at RHIC energies, and they are not visible inside the experimental error bars.

5 K^* -meson production on nuclear targets at LHC energies

In this section we will consider the K^{*0} and \bar{K}^{*0} -meson production in proton-nucleus and nucleus-nucleus collisions at LHC energies.

In the case of production of such particles as pions and kaons, which give the main contribution to mean multiplicity at RHIC energies, the shadowing effects already appear at RHIC [18]. In the case of K^* -meson production, as well as in the case of φ -meson production [4], the inelastic shadowing effects only appear at LHC energies. This behaviour can be connected with the relatively large mass of K^* . The inelastic shadowing effects for pions and kaons were experimentally confirmed by PHoBOS and PHENIX collaborations [42, 43, 44].

These saturation effects can be explained by the inelastic screening corrections due to the multipomeron interactions [18]. These corrections are negligibly small at low energies because of the suppression of the longitudinal part of nuclear form factor, but as this suppression of the longitudinal part of the nuclear form factor disappears with the growth of the initial energy, the inelastic screening corrections become more and more significant as the initial energy increases.

The calculations of inclusive densities and multiplicities, both in pA [45, 46], and in heavy ion collisions [46, 47], with accounting for inelastic nuclear screening, can be performed in the percolation approach, and they result in a good agreement with the experimental data for a wide energy range.

The percolation approach assumes two or several Pomerons to overlap in the transverse space and to fuse in a single Pomeron. Given a certain transverse radius, when the number of Pomerons in the interaction region increases, at least part of them may appear inside another Pomeron. As a result, the internal partons (quarks and gluons) can split, leading to the saturation of the final inclusive density. This effect persists with the energy growth until all the Pomerons will overlap [48, 49, 50].

In order to account for the percolation effects in the QGSM, it is technically more simple [44] to consider the maximal number of Pomerons n_{max} emitted by one nucleon

in the central region. After they are cut, these Pomerons lead to the different final states. Then the contributions of all the diagrams with $n \leq n_{max}$ are included into the analysis, as at lower energies. According to the unitarity constraint, a larger number of Pomerons $n > n_{max}$ can be emitted, but due to fusion in the final state (on the quark-gluon string stage) the cut of $n > n_{max}$ Pomerons results in the same final state as the cut of n_{max} Pomerons.

Here, n_{max} is a free parameter determined for K^* -meson production by comparison with experimental data at LHC energies, that it seems can be energy dependent [51].

In Table 4 we present the experimental data by the ALICE Collaboration for the production density dn/dy of average $K^{*0} = (K^{*0} + \bar{K}^{*0})/2$ mesons in the rapidity range $-0.5 \leq y \leq 0.5$ in $Pb + Pb$ collisions at $\sqrt{s} = 2.76$ TeV, for centrality 0-5% [37] and 0-20% [52], together with the non-single diffraction (NSD) data for K^{*0} -meson production in $p + Pb$ collisions at $\sqrt{s} = 5.02$ TeV [53], together with the results of the corresponding QGSM calculations.

Reaction	Centrality	Energy \sqrt{s} (TeV)	Experimental data $dn/dy, y \leq 0.5$	QGSM	QGSM no screening
$Pb + Pb \rightarrow K^{*0} + X$	0 - 5%	2.76	19.56 ± 2.64 [37]	20.1	48.83
$Pb + Pb \rightarrow K^{*0} + X$	0 - 20%	2.76	16.6 ± 2.57 [52]	16.6	44.00
$p + Pb \rightarrow K^{*0} + X$	NSD	5.02	0.315 ± 0.026 [53]	0.312	0.56

Table 4: Experimental data on $dn/dy, |y| \leq 0.5$ of average neutral $K^{*0} = (K^{*0} + \bar{K}^{*0})/2$ meson production in central $Pb + Pb$ and NSD $p + Pb$ collisions at LHC energies, together with the results of the corresponding QGSM calculations.

For the energy $\sqrt{s} = 2.76$ TeV, the model calculation correctly describes the experimental data on density dn/dy for average K^{*0} production in $Pb + Pb$ collisions [37, 52] for both centralities with a value $n_{max} = 30$. The calculations without screening corrections (infinite n_{max}), provide values for the density dn/dy significantly higher than the experimental ones, as it is shown in the last column of Table 4.

The calculated density $dn/dy, -0.5 \leq y \leq 0$ for $p + Pb$ collisions at $\sqrt{s} = 5.02$ TeV [53] corresponds to $n_{max}=31$. The experimental point on minimum bias spectrum has been normalised to the number of non-single-diffractive (NSD) events. The NSD events include double-diffractive interactions, where both nucleons break-up producing particles separated by a large rapidity gap, and other inelastic interactions.

In the case of pp collisions at $\sqrt{s} = 900$ GeV, the difference between NSD and all inelastic events is smaller than 15%, and this difference should be significantly smaller in proton-nucleus collisions. Thus, in the two-channel model this difference is only

about 3% [28]. We can then neglect this difference already in proton-nucleus collisions, so in Table 4 we compare the experimental data on NSD collisions with our calculations for all inelastic collisions.

The calculation of the density dn/dy with infinitely large n_{max} , that corresponds to the absence of shadowing, gives much higher values for K^{*0} production, both in $p + Pb$ collisions, as in $Pb + Pb$ collisions.

6 Conclusion

The QGSM provides a reasonable description of K^* -meson production for hadron-proton, proton-nucleus, and nucleus-nucleus interactions at not very high (up to RHIC) energies, without adding any new parameters with respect to the theoretically based (not free) parameters used to obtain the corresponding description of pion and kaon production.

The QGSM predictions for the A-dependences of K^* -meson production at $\sqrt{s} = 41$ GeV have the usual behaviour $d\sigma/dy(y=0) \propto A^1$, as it is shown in Fig. 8.

In this paper we show that the dependence of K^* -meson production on the initial energies in the midrapidity region differs from the case of production of light hadrons, as pions and kaons, since for K^* -mesons these inelastic screening effects are weaker and not visible inside the experimental error bars, up to the RHIC energies.

To include the inelastic shadowing contribution in the analysis of K^* -meson production, a new parameter n_{max} , determined by comparison with experimental data (see Section 5), is used.

Finally, we show that the inelastic screening effects for the case of K^* -meson production only begin to be visible at LHC energies, where we quantitatively estimate their importance.

This work has been supported by Russian grant RSGSS-3628.2008.2, by Ministerio de Ciencia e Innovación of Spain under project FPA2017-83814-P, and Maria de Maeztu Unit of Excellence MDM-2016-0692, and by Xunta de Galicia, Spain, under 2015-AEFIS (2015-PG034), AGRUP2015/11.

References

- [1] A.B. Kaidalov and K.A. Ter-Martorisyan, Sov. J. Nucl. Phys. **39**, 979 (1984) and Yad. Fiz. **39**, 1545 (1984).
- [2] A.B. Kaidalov, Phys. At. Nucl. **66**, 1994 (2003), doi:10.1134/1.1625743, and Yad. Fiz., **66**, 2044 (2003).

- [3] G.H. Arakelyan, C. Merino, and Yu.M. Shabelski, Phys. Rev. **D90**, 114019 (2014), doi:10.1103/PhysRevD.95.074013, and arXiv:1604.01918[hep-ph].
- [4] G.H. Arakelyan, C. Merino, and Yu.M. Shabelski, Phys. At. Nucl. **80**, 1197 (2017), 10.1134/S1063778817060035; Yad. Fiz. **80**, 719 (2017); and arXiv:1610.06039[nucl-th].
- [5] A.B. Kaidalov, K.A. Ter-Martirosyan, and Yu.M. Shabelski, Sov. J. Nucl. Phys. **43**, 822 (1986) and Yad. Fiz. **43**, 1282 (1986).
- [6] Yu.M. Shabelski, Z. Phys. **C38**, 569 (1988), doi:10.1007/BF01624362.
- [7] Yu.M. Shabelski, Sov. J. Nucl. Phys. **50**, 149 (1989) and Yad. Fiz. **50**, 239 (1989).
- [8] G.H. Arakelyan, C. Merino, C. Pajares, and Yu.M. Shabelski, Phys. At. Nucl. **76**, 316 (2013), doi:10.1134/S1063778813020026, Yad. Fiz. **76**, 348 (2013), and arXiv:1207.6899[hep-ph].
- [9] A.B. Kaidalov, O.I. Piskunova, Z. Phys. **C30**, 145 (1986), doi:10.1007/BF01560688.
- [10] Yu.M. Shabelski, Sov. J. Nucl. Phys. **44**, 117 (1986) and Yad. Fiz. **44**, 186 (1986).
- [11] G.H. Arakelyan, C. Merino, C. Pajares, and Yu.M. Shabelski, Eur. Phys. J. **C54**, 577 (2008), doi:10.1140/epjc/s10052-008-0554-1, and arXiv:0709.3174[hep-ph].
- [12] G.H. Arakelyan, C. Merino, C. Pajares, and Yu.M. Shabelski, Eur. Phys. J. **A31**, 519 (2007), doi:10.1140/epja/i2006-10282-6, and arXiv:0610.264[hep-ph].
- [13] G.H. Arakelyan, Sh.S. Eremian, Phys. At. Nucl. **58**, 1241 (1995) and Yad. Fiz. **58**, 1321 (1995).
- [14] G.H. Arakelyan, C. Pajares, and Yu.M. Shabelski, Z. Phys. **C73**, 697 (1997), doi:10.1007/s002880050361, and hep-ph/9602348.
- [15] M. Aguilar-Benitez *et al.*, Z. Phys. **C44**, 531 (1989), doi:10.1007/BF01549075.
- [16] N.M. Aghababyan *et al.*, Z. Phys. **C46**, 387 (1990), doi:10.1007/BF01621026.
- [17] G.G. Arakelian, A.A. Grigoryan, N.Ya. Ivanov, and A.B. Kaidalov, Z. Phys. **C63**, 137 (1994), doi:10.1007/BF01577553.
- [18] A. Capella, A. Kaidalov, and J. Tran Thanh Van, Acta Physica Hungarica-Heavy Ion Phys. **A9**, 169 (1999), and hep-ph/9903244.
- [19] G.H. Arakelyan, C. Merino, Yu.M. Shabelski, and A.G. Shuvaev, Phys. Rev. **D95**, 074013 (2017), doi:10.1103/PhysRevD.95.074013, and arXiv:1604.01918[hep-ph].

- [20] G.H. Arakelyan, A. Capella, A.B. Kaidalov, and Yu.M. Shabelski, Eur. Phys. J. **C26**, 81 (2002), doi:10.1007/s10052-002-0977-z, and arXiv:0103.337[hep-ph].
- [21] C. Merino, C. Pajares, and Yu.M. Shabelski, Eur. Phys. J. **C73**, 2266 (2013).
- [22] G.H. Arakelyan, C. Merino, and Yu.M. Shabelski, Eur. Phys. J. **A52**, 9 (2016), doi:10.1140/epja/i2016-16009-2, and arXiv:1509.05218[hep-ph].
- [23] V.A. Abramovsky, V.N. Gribov, and O.V. Kancheli, Sov. J. Nucl. Phys. **18**, 308 (1974); Yad. Fiz. **18**, 595 (1973).
- [24] A.B. Kaidalov, Sov. J. Nucl. Phys. **45**, 902 (1987) and Yad. Fiz. **45**, 1452 (1987).
- [25] A.B. Kaidalov and O.I. Piskounova, Sov. J. Nucl. Phys. **41**, 816 (1985) and Yad. Fiz. **41**, 1278 (1985).
- [26] A.A. Grigoryan, N.Ya. Ivanov, Sov. J. Nuc. Phys. **43**, 442 (1986) and Yad. Fiz. **43**, 693 (1986).
- [27] Yu.M. Shabelski, Z. Phys. **C57**, 409 (1993), doi:10.1007/BF01474336.
- [28] Yu.M. Shabelski, Sov. J. Nucl. Phys. **26**, 573 (1977) and Yad. Fiz. **26**, 1084 (1977); Nucl. Phys. **B132**, 491 (1978), doi:10.1016/0550-3213(78)90473-X.
- [29] L. Bertocchi and D. Treleani, J. Phys. **G3**, 147 (1977), doi:10.1088/0305-4616/3/2/007.
- [30] J.H. Weis, Acta Phys. Polonica **B7**, 851 (1976).
- [31] T. Jaroszewicz *et al.*, Z. Phys. **C1**, 181 (1979), doi:10.1007/BF01445409.
- [32] J. Dias de Deus and Yu.M. Shabelski, Phys. At. Nucl. **71**, 190 (2008) and Yad. Fiz. **71**, 191 (2008), doi:10.1007/s11450-008-1021-z,10.1134/S1063778808010213, and hep-ph/0612346.
- [33] G.D. Alkhasov *et al.*, Nucl. Phys. **A280**, 330 (1977), doi:10.1016/0375-9474(77)90609-1.
- [34] T. Anticic *et al.*, NA49 Collaboration, Phys. Rev. **C84**, 064909 (2011), doi:10.1103/PhysRevC.84.064909, and arXiv:1105.3109[nucl-ex].
- [35] M.Aguilar-Benitez *et al.*, LEBC-EHS Collaboration, Z. Phys. **C50**, 405 (1991), doi:10.1007/BF01551452.
- [36] J. Adams *at al.*, STAR Collaboration, Phys. Rev. **C 71**, 064902 (2005), doi:10.1103/PhysRevC.71.064902, and nucl-ex/0412019.
- [37] J. Adam *et al.*, ALICE Collaboration, Phys. Rev. **C95**, 064606 (2017), doi:10.1103/PhysRevC.95.064606, and arXiv:1702.00555[nucl-ex].

- [38] B. Abelev *et al.*, ALICE Collaboration, Eur. Phys. J. **C72**, 2183 (2012), doi:10.1140/epjc/s10052-012-2183-y, and arXiv:1208.5717[hep-ex].
- [39] I. Abt *et al.*, HERA-B Collaboration, Eur. Phys. J. **C50**, 315 (2007), doi:10.1140/epjc/s10052-007-0237-3, and hep-ex/0606049.
- [40] M.M. Aggarwal *et al.*, STAR Collaboration, Phys. Rev. **C 84**, 034909 (2011), doi:10.1103/PhysRevC.84.034909, and arXiv:1006.1961[nucl-ex].
- [41] C. Adler *at al.*, STAR Collaboration, Phys. Rev. **C 66**, 061901 (2002), doi:10.1103/PhysRevC.66.061901, and nucl-ex/0205015.
- [42] B.B. Back *et al.*, PHOBOS Collaboraboration, Phys. Rev. Lett. **85**, 3100 (2000), doi:10.1103/PhysRevLett.85.3100, and hep-ex/0007036.
- [43] K. Adcox *at al.*, PHENIX Collaboration, Phys. Rev. Lett. **86**, 3500 (2001), doi:10.1103/PhysRevLett.86.3500, and nucl-ex/0012008.
- [44] C. Merino, C. Pajares, and Yu.M. Shabelski, Eur. Phys. J. **C59**, 691 (2009), doi:10.1140/epjc/s10052-008-0810-4, and arXiv:0802.2195[hep-ph].
- [45] I. Bautista, C. Pajares, and J. Dias de Deus, Nucl. Phys. **A882**, 44 (2012), doi:10.1016/j.nuclphysa.2012.03.003, and arXiv:1110.4740[nucl-th].
- [46] I. Bautista, J. Dias de Deus, G. Milhano, and C. Pajares, Phys. Lett. **B715**, 230 (2012), doi:10.1016/j.physletb.2012.07.029, and arXiv:1204.1457[nucl-th].
- [47] I. Bautista, C. Pajares, G. Milhano, and J. Dias de Deus, Phys. Rev. **C86**, 034909 (2012), doi:10.1103/PhysRevC.86.034909, and arXiv:1206.6737[nucl-th].
- [48] J. Dias de Deus, E. G. Ferreira, C. Pajares, and R. Ugoccioni, Eur. Phys. J. **C40**, 229 (2005), doi:10.1140/epjc/s2005-02127-y, and hep-ph/0304068.
- [49] C. Pajares, Eur. Phys. J. **C43**, 9 (2005), doi:10.1140/epjc/s2005-02179-y, and hep-ph/0501125.
- [50] M.A. Braun, E.G. Ferreira, F. del Moral, and C. Pajares, Eur. Phys. J. **C25**, 249 (2002), doi:10.1007/s10052-002-0989-8, and hep-ph/0111378.
- [51] M.A. Braun, C. Pajares, Eur. Phys. J. **C16**, 349 (2000), doi:10.1007/s100520050027; M.A. Braun, R.S. Kolevatov, C. Pajares, V.V. Vechernin, Eur. Phys. J. **C32**, 535 (2004), DOI: 10.1140/epjc/s2003-01443-6
- [52] B. Abelev *et al.*, ALICE Collaboration, Phys. Rev. **C91**, 024609 (2015), doi:10.1103/PhysRevC.91.024609, and arXiv:1404.0495[nucl-ex].
- [53] J. Adam *et al.*, ALICE Collaboration, Eur. Phys. J. **C76**, 245 (2016), doi:10.1140/epjc/s10052-016-4088-7, and arXiv:1601.07868.